Published in final edited form as:

JACC Cardiovasc Imaging. 2018 February ; 11(2 Pt 2): 320–332. doi:10.1016/j.jcmg.2017.11.019.

Feasibility Evaluation of Myocardial Cannabinoid Type 1 Receptor Imaging in Obesity:

A Translational Approach

Ines Valenta, MD[a], **Zoltan V. Varga, MD, PHD**[b], **Heather Valentine, PHD**[a], **Resat Cinar, PHD**[c], **Andrew Horti, PHD**[a], **William B. Mathews, PHD**[a], **Robert F. Dannals, PHD**[a], **Kimberley Steele, MD**[d], **George Kunos, MD, PHD**[c], **Richard L. Wahl, MD**[e], **Martin G. Pomper, MD, PHD**[a], **Dean F. Wong, MD, PHD**[a], **Pal Pacher, MD, PHD**[b], and **Thomas H. Schindler, MD**[a]

[a]Department of Radiology, Division of Nuclear Medicine, Nuclear Cardiovascular Medicine, Johns Hopkins University School of Medicine, Baltimore, Maryland; [b]Laboratory of Cardiovascular Physiology and Tissue Injury, National Institute on Alcohol Abuse and Alcoholism, National Institutes of Health, Bethesda, Maryland; [c]Laboratory of Physiological Studies, National Institute on Alcohol Abuse and Alcoholism, National Institutes of Health, Bethesda, Maryland; [d]Department of Surgery, Bariatric Center at Bayview, Johns Hopkins University School of Medicine, Baltimore, Maryland; [e]Washington University School of Medicine, Mallinckrodt Institute of Radiology, St. Louis, Missouri.

Abstract

OBJECTIVES—The aim of this study was to evaluate the feasibility of targeted imaging of myocardial cannabinoid type 1 receptor (CB1-R) and its potential up-regulation in obese mice with translation to humans using [^{11}C]-OMAR and positron emission tomography (PET)/computed tomography (CT).

BACKGROUND—Activation of myocardial CB1-R by endocannabinoids has been implicated in cardiac dysfunction in diabetic mice. Obesity may lead to an up-regulation of myocardial CB1-R, potentially providing a mechanistic link between obesity and the initiation and/or progression of cardiomyopathy.

METHODS—Binding specificity of [^{11}C]-OMAR to CB1-R was investigated by blocking studies with rimonabant in mice. The heart was harvested from each mouse, and its radioactivity was determined by γ-counter. Furthermore, [^{11}C]-OMAR dynamic micro-PET/CT was carried out in obese and normal-weight mice. Ex vivo validation was performed by droplet digital polymerase chain reaction (absolute quantification) and RNAscope Technology (an in situ ribonucleic acid analysis platform). Subsequently, myocardial CB1-R expression was probed noninvasively with

ADDRESS FOR CORRESPONDENCE: Dr. Thomas Hellmut Schindler, Johns Hopkins University, School of Medicine, Division of Nuclear Medicine, Cardiovascular Nuclear Medicine, Department of Radiology and Radiological Science SOM, JHOC, 3225 601 North Caroline Street, Baltimore, Maryland 21287., tschind3@jhmi.edu. OR Dr. Pal Pacher, Laboratory of Cardiovascular Physiology and Tissue Injury, National Institutes of Health/NIAAA, 5625 Fishers Lane, MSC-9413, Bethesda, Maryland 20892-9413., pacher@mail.nih.gov.

Drs. Valenta and Varga contributed equally to this paper and are joint first authors. Drs. Pacher and Schindler contributed equally to this work and are joint senior authors.

APPENDIX For supplemental methods and a figure, please see the online version of this paper.

intravenous injection of CB1-R ligand [^{11}C]-OMAR and PET/CT in humans with advanced obesity and normal-weight human control subjects, respectively.

RESULTS—Rimonabant significantly blocked OMAR uptake in the heart muscle compared with vehicle, signifying specific binding of OMAR to the CB1-R in the myocardium. The myocardial OMAR retention quantified by micro-PET/CT in mice was significantly higher in obese compared with normal-weight mice. Absolute quantification of CB1-R gene expression with droplet digital polymerase chain reaction and in situ hybridization confirmed CB1-R up-regulation in all major myocardial cell types (e.g., cardiomyocytes, endothelium, vascular smooth muscle cells, and fibroblasts) of obese mice. Obese mice also had elevated myocardial levels of endocannabinoids anandamide and 2-arachidonoylglycerol compared with lean mice. Translation to humans revealed higher myocardial OMAR retention in advanced obesity compared with normal-weight subjects.

CONCLUSIONS—Noninvasive imaging of cardiac CB1-R expression in obesity is feasible applying [^{11}C]-OMAR and PET/CT. These results may provide a rationale for further clinical testing of CB1-R-targeted molecular imaging in cardiometabolic diseases.

Keywords

anandamide; cannabinoid type 1 receptor; CB1 receptor imaging; [^{11}C]-OMAR; endocannabinoids; heart; obesity; PET/CT; 2-arachidonoylglycerol

---

In recent decades there has been a continuous rise in the prevalence of obesity in industrialized nations, reaching ≥30%; strikingly, up to about 6% to 8% of the population may even have morbid obesity, with a body mass index (BMI) ≥40 kg/m^2 (1). As epidemiological investigations have demonstrated that obesity constitutes an important risk factor of cardiovascular morbidity and mortality, the increasing prevalence of obesity may become a pivotal public health concern (1,2). Although standard medical treatment of patients with heart failure with beta-blockers, angiotensin-converting enzyme inhibitors, angiotensin II type 1 receptor blockers, and aldosterone antagonists beneficially affects morbidity and mortality, the 5-year mortality rate for patients with heart failure remains high at 50% (3). The exact mechanisms by which obesity initiates and accelerates cardiovascular disease, however, are still elusive. Obesity has been demonstrated as an independent predictor of coronary circulatory dysfunction that is considered an early functional precursor of the coronary artery disease process (4,5). It has been suggested that increases in adipose-derived and locally synthetized endocannabinoids in the cardiovascular system and also macrophages may not only exert proatherosclerotic effects (4,6), favoring the development of coronary artery disease but also promote cardiac dysfunction in diabetes via cannabinoid type 1 receptor (CB-1 R) signaling (7). Activation of myocar-dial CB1-R by endocannabinoids and synthetic cannabinoids is likely to induce cardiac dysfunction via mitogen-activated protein kinase activation, angiotensin II type 1 receptor expression and signaling, advanced glycation end product accumulation, oxidative and nitrative stress, inflammation, and fibrosis, as shown in diabetic mice and in rats with chronic ischemic heart failure (6,7). In view of this and a dysregulated endocannabinoid system in obesity (6), it is intriguing to speculate that pronounced increases in body weight may modulate myocardial CB1-R expression, potentially providing a mechanistic link between obesity and the initiation of cardiomyopathy. The dramatic increase in reported severe cardiovascular effects

of marijuana and synthetic cannabinoids during the past few years also calls for research to a better understanding of the role of human cardiac CB1-R (6).

To this end, we aimed to evaluate the feasibility of targeted imaging of myocardial CB1-R and its potential up-regulation in obese mice with translation to humans using [^{11}C]-OMAR and positron emission tomography (PET)/computed tomography (CT).

METHODS

BIODISTRIBUTION STUDIES WITH [^{11}C]-OMAR.

These studies were performed as described in detail in the supplemental methods.

RADIOSYNTHESIS OF [^{11}C]-OMAR, BIODISTRIBUTION, AND MICRO-PET/CT IN MICE.

The synthesis of [^{11}C]-OMAR ([^{11}C]JHU75528), a CB1-R-selective positron emission tomographic radioligand structurally similar to the CB1-R inverse agonist rimonabant (Figure 1), was performed in our laboratory as previously described (8). The animal study protocol was approved by the Johns Hopkins Institutional Animal Care and Use Committee. The investigated mice were handled according to the principles of the American Physiological Society. All animal positron emission tomographic/computed tomographic studies in lean male (23 to 31 g) C57Bl/6J mice (wild type) and in obese (35 to 63 g) age-matched ob/ob homozygous mice on a C57Bl/6J background were conducted and analyzed in the Johns Hopkins University small-animal imaging suite, as detailed in the Online Appendix and previously described (9–11). At the conclusion of imaging, anesthetized mice were euthanized, hearts were quickly perfused and excised and immediately frozen and stored at 80°C for consequent ribonucleic acid (RNA) isolation and biochemical measurements.

RNA isolation, complementary deoxyribonucleic acid synthesis, droplet digital polymerase chain reaction (PCR), western blot, histology and immunohistochemistry, myocardial endocannabinoid content measurements, and RNA in situ hybridization for the detection and cell type–specific expression of myocardial CB1 messenger RNA transcripts using RNAscope Technology (Advanced Cell Diagnostics, Newark, California) were described previously (6,7) and/or detailed in the Online Appendix.

HUMAN APPLICATION OF [^{11}C]-OMAR.

The study population comprised 12 healthy study participants without arterial hypertension, smoking, hypercholesterolemia, or diabetes mellitus, as outlined in Table 1. Of these, 7 subjects had advanced obesity (AOB) (BMI ≥38 kg/m^2), while 5 normal-weight participants served as control subjects (CON) (BMI <25 kg/m^2). Study applicants had been recruited using flyers and newspaper advertisements. A study prerequisite was the absence of any cardiovascular, systemic disease, or cannabis use. Study participants underwent an initial screening visit that included a physical examination, electrocardiogram, blood pressure measurements, and routine blood chemistry. Physical examination revealed normal findings in all study participants, and they had normal results on resting electrocardiography. Subsequently, each study participant underwent ^{13}N-ammonia and [^{11}C]-OMAR PET/CT

(64-slice Discovery Rx VCT, GE Healthcare, Little Chalfont, United Kingdom) to noninvasively assess myocardial flow at rest and CB1-R expression. BMI was calculated as weight (kilograms) divided by the square of height (meters). Routine blood chemistry included plasma glucose, total cholesterol, high-density lipoprotein and low-density lipoprotein cholesterol, triglyceride, and high-sensitivity C-reactive protein. The study was approved by the Johns Hopkins Institutional Review Board (00050595), and each study participant signed the approved informed consent form.

PET AND MYOCARDIAL PERFUSION ASSESSMENT.

Resting myocardial perfusion and myocardial blood flow in milliliters per gram per minute were determined as detailed in the Online Appendix and previously described (12).

PET AND MYOCARDIAL CB1-R IMAGING.

Synthesis of [^{11}C]-OMAR ([^{11}C]JHU75528), a CB1-R-selective positron emission tomographic radioligand, was performed as described previously (8). Following a slow-bolus injection of about 740 MBq [^{11}C]-OMAR, serial positron emission tomographic image acquisition (12 × 10, 3 × 20, 2 × 60, 2 × 150, 2 × 300, and 2 × 600 s) and a 40-min static scan were performed. For quantitative analysis, the left ventricular contouring was positioned on the summed dynamic data and projected to the dynamic frames. Furthermore, the arterial input function and spillover were defined by a region of interest into the left and right ventricles, respectively, and time-activity curves were obtained. The tracer kinetic model applied, corrected for radiotracer decay, partial volume–related underestimation of true myocardial tissue concentrations, and spillover of radioactivity between the left ventricular blood pool and myocardium (12). From the arterial input function and time-activity curves from all 23 dynamic frames, the myocardial retention index of OMAR (OMAR-ret) as a percentage per minute was determined (11). Regional OMAR-ret of the left anterior descending, left circumflex, and right coronary artery territories was averaged on a polar map, and the resulting mean OMAR-ret was defined as global OMAR-ret of the left ventricle. Heart rate, blood pressure, and a 12-lead electrocardiogram were recorded continuously during OMAR-ret measurement. Venous blood was taken at 10 and 40 min to determine plasma metabolites by column-switch high-performance liquid chromatography (8).

STATISTICAL ANALYSIS.

Because continuous variables are not always normally distributed, they are presented as median and range (lowest and highest value). For comparison of differences, we used the Mann-Whitney *U* test for independent samples (SPSS Statistics version 22.0, IBM, Armonk, New York). A comparison of differences in OMAR-ret among the 3 major vascular coronary territories was performed by Friedman analysis of variance by ranks for the paired analysis of vessel area. For other variables, repeated-measures analysis of variance or unpaired Student *t* tests were used as appropriate. Statistical significance was assumed if the null hypothesis could be rejected at $p < 0.05$.

RESULTS

BIODISTRIBUTION OF [^{11}C]-OMAR IN OBESE MICE.

After intravenous injection of [^{11}C]-OMAR in the obese mice, the highest accumulation was seen in the heart, followed by the cerebellum, thalamus, and blood at 5 min (Table 2, Figure 2A). This pattern of [^{11}C]-OMAR signal remained similar between 5 and 15 min for the heart, cerebellum, thalamus, and blood. This was followed by some decline in the [^{11}C]-OMAR uptake pattern in examined brain regions and blood at 30 min, while the accumulation in the heart was comparable with that in the cerebellum. Between 30 and 90 min, the accumulation pattern of examined heart, brain regions, and blood remained widely constant. To provide proof of CB1-R receptor specificity of the [^{11}C]-OMAR in the obese mouse heart, a blocking study with rimonabant was performed over a 5-min period. Table 3 and Figure 2B illustrate CB1-R binding specificity of [^{11}C]-OMAR with dose escalation of 1 and 5 mg/kg rimonabant blocking. As can be appreciated, the CB1-R inhibitor rimonabant blocked [^{11}C]-OMAR in selected studied brain regions of the cerebellum and thalamus in a dose-dependent fashion, while to block [^{11}C]-OMAR in the blood pool, 5 mg/kg rimonabant was necessary. At the low dose of 1 mg/kg rimonabant, there were reductions of [^{11}C]-OMAR uptake in the cerebellum and thalamus by 38% and 25%, respectively, compared with corresponding vehicle. At the highest blocker dose of 5 mg/kg, however, the reduction of [^{11}C]-OMAR uptake in the cerebellum and thalamus increased to 68%, respectively. Conversely, 1 mg/kg of rimonabant was not sufficient to block the signal from [^{11}C]-OMAR in the blood and the heart compared with vehicle, but rather paradoxical increases in the signal of 67% and 10%, respectively, were observed, likely related to the peripheral blocking effects of rimonabant with increased [^{11}C]-OMAR blood radioactivity and, correspondingly, myocardial uptake in conjunction with insufficient myocardial blocking effects of low-dose rimonabant. Conversely, increasing the dose of rimonabant to 5 mg/kg did block [^{11}C]-OMAR uptake in the blood and myocardium by 55% and 58%, respectively, compared with vehicle.

[^{11}C]-OMAR AND PET/CT IN MICE.

Myocardial OMAR was clearly detectable and regionally homogenous in mice (Figure 2C). There was strong liver uptake of OMAR that widely did not interfere with myocardial visualization, as long as it was not overlapping with the inferoseptal and inferior wall. In 2 obese mice, adjacent and overlapping OMAR uptake of the liver with the myocardium of the inferoseptal and inferior was noted, and the evaluation of OMAR uptake thereof was excluded from analysis. In addition, in 2 normal-weight mice, [^{11}C]-OMAR injection into the tail vein failed. Quantification of myocardial OMAR retention in the remaining mice, however, proved to be significantly higher in obese than in normal-weight mice (8.29%/min [2.12%/min to 15.14%/min] vs. 0.13%/min [0.00%/min to 0.16%/min]; $p \leq 0.009$) (Figures 2C and 2D), indicating myocardial CB1-R up-regulation in obese mice. In this respect, the binding potential of [^{11}C]-OMAR to myocardial CB1-R in obese mice proved to be 6.4, emphasizing the usefulness of this radio-ligand to image myocardial CB1-R expression.

MYOCARDIAL CB1-R EXPRESSION AND ENDOCANNABINOID LEVELS IN MICE.

Absolute quantification of myocardial CB1-R gene expression by droplet digital PCR showed up-regulation of CB1-R but not cannabinoid type 2 receptor (CB2-R) in obese versus lean mice (Figures 3A to 3C), with an increase in [^{11}C]-OMAR retention in obese mice (Figure 2D). To visualize the change in messenger RNA expression, we also performed RNA in situ hybridization, which showed a marked myocardial increase of the CB1-R transcript in obese hearts (Figures 3D to 3F). CB1-R transcript was expressed in endothelial cells, as shown by colocalization with the endothelial marker Pecam1-CD31 (Figure 4A); it was present in the vascular smooth muscular layer of vessels (detected by the marker Sm22α) (Figure 4B); and also colocalized with the cardiomyocyte-specific marker cardiac troponin T (Figure 5A) and with the fibroblast marker vimentin (Figure 5B). We also attempted to localize myocardial CB1-R with the 5 most commonly used CB1-R antibodies (both C- and N-terminal specific) and first tested these with both positive and negative control subjects (cerebellum from wild-type and CB1-R-knockout mice) (Online Figures 1A to 1F). Surprisingly, all CB1-R antibodies presented multiple bands on western blots, mostly not even at expected molecular weights. All these bands were also present in CB1-R-knockout mice with confirmed genotype (Online Figures 1A to 1G), indicating nonspecificity of antibodies.

In addition, we identified significantly increased levels of myocardial endocannabinoids such as anandamide and 2-arachidonoylglycerol in obese compared with lean mice, which may account for activation of the CB1-R, indicating not only increased expression but subsequent ligand-dependent activation of CB1-R signaling (Figures 6A and6B). We also found a marked increase in cardiac arachidonic acid level, implying an increased metabolic turnover of endocannabinoids, which likely contributes to a proinflammatory milieu (Figure 6C). Cyclooxygenase-2 showed increased myocardial protein expression in obese mice (Figures 6D and6E), signifying subsequent metabolism of arachidonic acid (e.g., to the lipid peroxidation product 4-hydroxynonenal) (Figure 6F), contributing to a proinflammatory and pro-oxidant milieu.

^{13}N-AMMONIA AND [^{11}C]-OMAR RETENTION IN HUMANS.

The clinical characteristics, laboratory measurements, and hemodynamic parameters during PET/CT among groups are demonstrated in Table 1. Resting ^{13}N-ammonia retention on positron emission tomographic/computed tomographic images was homogeneous in all study participants. Arterial blood pressures and heart rate were nonsignificantly elevated in AOB compared with CON. At rest, myocardial blood flow was also higher in AOB than in CON, not reaching statistical significance (Table 1). Furthermore, when adjusted for rate-pressure product, normalized myocardial blood flow also tended to be higher in AOB than in CON, while coronary vascular resistance was comparable. With respect to the visualization of myocardial CB1-R with [^{11}C]-OMAR, there was a widely homogenous signal throughout the left ventricle in AOB and CON on normalized images (Figure 7A). Absolute left ventricular retention of [^{11}C]-OMAR was significantly higher in AOB than in CON (5.68%/min [1.88%/min to 6.89%/min] vs. 0.47%/min [0.13%/min to 1.31%/min]; $p \leq 0.006$) (Figures 7A and7B), indicative of myocardial CB1-R up-regulation in AOB. Notably, plasma metabolite analysis demonstrated relative radiotracer stability in 2 CON and AOB,

respectively (92% [90% to 93%] and 91% [89% to 94%] at 10 min after injection and 17% [16% to 18%] and 18% [17% to 20%] at 40 min), outlining comparable radio-tracer conditions between groups. Furthermore, we investigated the regional OMAR-ret according to the 3 major coronary artery territories. Although for CON, no significant differences of the OMAR-ret among vascular regions were noted (0.28%/min [0.04%/min to 1.24%/min] vs. 0.43%/min [0.06%/min to 1.79%/min] vs. 0.24%/min [0.07%/min to 1.53%/min]; $p = 0.247$), significant heterogeneity in its uptake was observed in AOB (4.49%/min [1.13%/min to 5.67%/min] vs. 5.51%/min [1.96%/min to 8.88%/min] vs.6.65%/min [3.10%/min to 7.78%/min]; $p \leq 0.018$ by Friedman analysis of variance by ranks).

DISCUSSION

The present translational study, using noninvasive in vivo imaging with [^{11}C]-OMAR and PET/CT and absolute quantification of myocardial CB1-R expression in mice with digital PCR and RNA in situ hybridization, for the first time provides proof of concept of an up-regulation of myocardial CB1-R in AOB in both mice and humans. The increased myocardial expression of CB1-R messenger RNA in obese mice was present in cardiomyocytes, endothelial cells, vascular smooth muscle cells, and fibroblasts. This was also associated with elevated levels of myocardial endocannabinoids (anandamide and 2-arachidonoylglycerol) in obese mice, signifying ligand-dependent activation of CB1-R signaling. The observed increase in cardiac arachidonic acid level provides evidence of increased metabolic turnover of endocannabinoids, likely adding to a proin-flammatory environment (6). Because activation of myocardial CB1-R by endocannabinoids may promote cell death, oxidative stress, proinflammatory response, and cardiac dysfunction (7,13), the noted up-regulation of myocardial CB1-R may raise the intriguing hypothesis of a mechanistic link between obesity and the initiation of cardiomyopathy that remains to be verified in further investigations.

[^{11}C]-OMAR, like other CB1-R radiotracers such as ^{18}[F]MK-9470, ^{18}[F]FMPEP-d2, ^{11}[C]MePPEP, and ^{11}[C] SD5024, has been applied to CB1-R imaging in the brain. Structurally, these positron emission tomographic radiotracers are related to the CB1-R inverse agonist rimonabant (SR141716) and possess high lipophilicity (14). The CB1-R affinity of [^{11}C]-OMAR ranges from K_i = 2.1 to 11 nmol/l (15); this affinity combined with the fast kinetics of [^{11}C]-OMAR allows shorter brain positron emission tomographic scans compared with other radiotracers, which commonly need 90 to 120 min of dynamic data. In the present investigation, we evaluated the feasibility of myocardial CB1-R expression imaging and quantification with [^{11}C]-OMAR PET/CT in obese mice. In this respect, the biodistribution time course of OMAR in the cerebellum, thalamus, blood, and heart was assessed. After intravenous injection of [^{11}C]-OMAR in the obese mice, there was a progressive decrease of OMAR binding from 5 to 30 min, settling to a lower plateau maintained constant up to 90 min. Such observations denote significant OMAR uptake in the obese mouse heart. Although the [^{11}C]-OMAR uptake in the brain has been demonstrated to bind specifically to the CB1-R (9), it could be speculated that the observed OMAR uptake in the obese mouse heart could be related to nonspecific myocardial uptake. To provide proof of CB1-R specificity of [^{11}C]-OMAR in the obese mouse heart, a blocking study with the CB1-R inverse agonist rimonabant was performed. It is important to note that rimonabant as

an inverse agonist of CB1-R typically changes the conformation of the receptor, thus preventing binding of endogenous ligands. This blocking mechanism of rimonabant is different from the classic competitive antagonism (15). As described in previous studies in mouse brain (9), we observed a marked reduction of OMAR uptake with peritoneal application of 5 mg/kg rimonabant of about 68% in the brain regions of both the cerebellum and thalamus, as well as 55% in the blood, in obese mice compared with control mice. Similarly, rimonabant application diminished the measured [^{11}C]-OMAR uptake in the mouse heart by about 58% compared with those without. Although this blocking of myocardial [^{11}C]-OMAR uptake is less than reported for brain studies, at about 75% (9), it may signify predominant CB1-R-specific binding of [^{11}C]-OMAR in the heart in obese mice. Furthermore, despite the observed lower specificity of [^{11}C]-OMAR uptake of the heart compared with the brain, it was sufficient to differentiate high myocardial [^{11}C]-OMAR uptake in obesity from relatively low uptake in lean control subjects in both mice and humans.

In the present myocardial blocking study of [^{11}C]-OMAR uptake, the baseline-to-block ratio was about 2.4, and correspondingly the binding potential was >1. A receptor binding potential of a radiotracer exceeding 1 is commonly deemed as suitable for quantification with PET (8). Previous blocking studies with [^{11}C]-OMAR in the brain (9) demonstrated a binding potential of about 2. The binding potential value depends on the receptor density in the organ or region of interest. In the brain, CB1-R density is among the greatest of all G protein–coupled receptors. Current results suggest that CB1-R density in the heart is lower than in the brain, but it is still sufficient for quantification. Yet about 42% of [^{11}C]-OMAR uptake could not be blocked by the 5 mg/kg dose of CB1-R antagonist rimonabant; suboptimal peritoneal resorption of rimonabant, early nonspecific [^{11}C]-OMAR binding, or interactions of the radioactive metabolites of [^{11}C]-OMAR with cannabinoid receptors may account for this. When analyzing [^{11}C]-OMAR uptake in the heart of genetically obese ob/ob mice and lean control mice of the same genetic background, we were able to detect 8-fold higher [^{11}C]-OMAR retention in the obese versus lean mice with [^{11}C]-OMAR and micro-PET/CT, which was supported by a parallel increase in CB1-R gene expression, quantified ex vivo by droplet digital PCR and visualization with RNAscope (in situ hybridization). Conversely, the pronounced uptake of [^{11}C]-OMAR in the liver may have contributed, at least in part, to an increased and heterogeneous myocardial signal when in proximity thereto. To overcome these limitations, efforts to develop a less lipophilic CB1-R radiotracer ligand with improved imaging characteristics are certainly warranted. Of further interest, the cardiac tissue levels of both endocannabinoids were also significantly higher in ob/ob compared with lean mice, which is in good agreement with human studies demonstrating that elevated endocannabinoid plasma levels were associated with coronary circulatory dysfunction in obesity (4,5). Increased production of endocannabinoids, together with the increased expression of their cognate receptors, could indicate increased myocardial CB1-R signaling.

Human studies in healthy volunteers also demonstrated that the cardiovascular effects of Δ^9−tetrahydrocannabinol (the psychoactive constituent of marijuana) could be reversed by 2 clinically used CB1-R antagonists (including rimonabant), indicating CB1-R involvement, and peripherally restricted CB1-R agonists for pain but they failed because of cardiovascular

side effects in these clinical trials (6). Furthermore, a large number of recent studies have linked the recreational use of synthetic designer cannabinoids (mixtures of very potent synthetic CB1-R agonists with potency up to 100 to 200 times that of Δ^9−tetrahydrocannabinol at CB1-R) to myocardial infarction, cardiomyopathies and heart failure, arrhythmias, stroke, and cardiac arrest, among other toxicities both in children and adults (6), supporting an important role of CB1-R in the cardiovascular system in humans.

Given the importance of CB1-R in the human cardiovascular system, we extended our mouse studies also to the human myocardium of subjects with normal weight and those with AOB and demonstrate the feasibility of targeted imaging of myocardial CB1-R using [^{11}C]-OMAR and PET/CT. It could be argued, however, that the observed increase in myocardial [^{11}C]-OMAR uptake in obesity could reflect a nonspecific response to a general systemic effect of obesity on the endocannabinoid system. Conversely, given the observed relatively high variability of myocardial [^{11}C]-OMAR uptake in obese subjects, [^{11}C]-OMAR and PET imaging could indeed prove to be unique tools to identify those obese subjects with relatively high myocardial CB1-R expression likely to develop cardiomyopathy and, importantly, who are likely to respond to preventive medical care with upcoming peripherally restricted CB1-R inverse agonists and neutral antagonists, which warrants further investigation.

Notably, all obese subjects had normal left ventricular function, as determined with ^{13}N-ammonia gated PET, so that the observed myocardial CB1-R expression in these subjects is unlikely to be secondary to compromised systolic left ventricular function. In contrast, because we did not perform echocardiography, we cannot entirely exclude that some mild left ventricular hypertrophy may have contributed, at least in part, to some alterations in CB1-R expression in AOB. In contrast, diastolic parameters as measured with gated PET proved to be within the normal range and comparable among groups, signifying the absence of significant diastolic dysfunction in AOB as a potential cause for the observed increased myocardial [^{11}C]-OMAR on positron emission tomographic/computed tomographic images. As described for previous pharmacokinetic studies for ligands targeting adreno- and muscarinic receptor, changes in flow and permeability may influence time-activity curves and thus myocardial [^{11}C]-OMAR uptake (16). In the present study, resting myocardial blood flow, as determined with ^{13}N-ammonia PET, tended to be higher in subjects with AOB compared with normal body weight, which might have contributed, at least in part, to increased myocardial [^{11}C]-OMAR uptake in subjects with AOB.

STUDY LIMITATIONS.

There are several limitations that need to be weighed in interpreting these findings. First, we cannot exclude a certain amount of nonspecific myocardial binding to CB1-R because of metabolism of OMAR that generated nonactive radiometabolites of [^{11}C]-OMAR. Although radio-metabolites are more polar than in the parent compound in humans, and there is at least 94% of radioactivity related to unchanged [^{11}C]-OMAR as reported in brain studies (8), the amount of radio-metabolite contamination of the PET-determined myocardial signal in the present study remains uncertain.

Second, we were not able to perform an ex vivo validation with histological analysis of myocardial CB1-R expression using the most widely applied antibodies in mice, because all antibodies we tested with positive and negative control subjects turned out to be nonspecific (Online Figure 1). However, we provide compelling evidence by showing that the micro-PET/CT–quantified myocardial OMAR-ret with an increase in obese versus lean mice was virtually mirrored by ex vivo measured CB1-R gene expression as a surrogate marker for myocardial CB1-R expression. Yet it is important to keep in mind that messenger RNA levels do not always correlate directly to receptor protein expression.

Third, although we demonstrate the feasibility [^{11}C]-OMAR and PET/CT to noninvasively probe myocardial CB1-R expression in subjects with AOB compared with lean control subjects, the feasibility and accuracy of this imaging approach to identify myocardial CB1-R expression in the “intermediate range” in subjects with overweight or mild to moderate obesity still needs to be determined.

Fourth, in view of the reported relatively modest affinity of [^{11}C]-OMAR to brain CB1-R (15), it remains to be seen whether this imaging approach is also sensitive enough to monitor treatment related alterations in myocardial CB1-R expressions. Furthermore, because we performed the [^{11}C]-OMAR and positron emission tomographic/computed tomographic imaging study only in male mice, additional studies also in female mice are needed to identify potential sex differences in myocardial CB1-R expression.

Finally, the ligand binding (extra- or intracellular domain) site of [^{11}C]-OMAR and its binding characteristics in the myocardial cells need further evaluation.

CONCLUSIONS

Noninvasive in vivo imaging of cardiovascular CB1-R expression with [^{11}C]-OMAR PET/CT is feasible, and it reveals marked up-regulation of myocardial CB1-R in obesity. These results may justify further clinical testing of CB1-R-targeted molecular imaging in cardiometabolic and possibly other cardiovascular diseases. The latter is also justified by reports on cardiomyopathies, myocardial infarction, and acute heart failure induced by synthetic cannabinoids, which may also alter CB1-R expression and function.

Supplementary Material

Refer to Web version on PubMed Central for supplementary material.

ACKNOWLEDGMENTS

The authors thank Corina Voicu and Jeannie Peters for assisting in the positron emission tomographic studies and the cyclotron staff for [^{11}C]-OMAR production. Furthermore, the authors are thankful to Valery Bliskovsky, Steve Shema, and Liz Conner (National Cancer Institute Center for Cancer Research Genomics Core) for their help with the droplet digital PCR measurements. Special acknowledgment is made to Lorena Gapasin for regulatory and human subjects approval assistance.

This work was supported by a Departmental Fund from Johns Hopkins University (175470 to Dr. Schindler) and the Intramural Research Program of National Institute on Alcohol Abuse and Alcoholism/National Institutes of Health (to Drs. Kunos and Pacher). Dr. Varga was supported by the Rosztoczy Foundation. All other authors have reported that they have no relationships relevant to the contents of this paper to disclose.

ABBREVIATIONS AND ACRONYMS

AOB	advanced obesity
BMI	body mass index
CB1-R	cannabinoid type 1 receptor
CB2-R	cannabinoid type 2 receptor
CON	control subjects
CT	computed tomography
EC	endocannabinoid
OMAR-ret	myocardial retention index of OMAR
PCR	polymerase chain reaction
PET	positron emission tomography
RNA	ribonucleic acid

REFERENCES

1. Flegal KM, Carroll MD, Kit BK, Ogden CL. Prevalence of obesity and trends in the distribution of body mass index among US adults 1999–2010. JAMA 2012;307:491–7. [PubMed: 22253363]
2. Dilsizian V, Zynda TK, Petrov A, et al. Molecular imaging of human ACE-1 expression in transgenic rats. J Am Coll Cardiol Img 2012;5:409–18.
3. Schindler TH, Dilsizian V. Cardiac positron emission tomography/computed tomography imaging of the renin-angiotensin system in humans holds promise for image-guided approach to heart failure therapy. J Am Coll Cardiol 2012;60:2535–8. [PubMed: 23158529]
4. Quercioli A, Montecucco F, Pataky Z, et al. Improvement in coronary circulatory function in morbidly obese individuals after gastric bypass-induced weight loss: relation to alterations in endocannabinoids and adipocytokines. Eur Heart J 2013;34:2063–73. [PubMed: 23487518]
5. Quercioli A, Pataky Z, Montecucco F, et al. Coronary vasomotor control in obesity and morbid obesity: contrasting flow responses with endocannabinoids, leptin, and inflammation. J Am Coll Cardiol Img 2012;5:805–15.
6. Pacher P, Steffens S, Hasko G, Schindler TH, Kunos G. Cardiovascular effects of marijuana and synthetic cannabinoids: the good, the bad and the ugly. Nat Rev Cardiol 2017 9 14 [E-pub ahead of print].
7. Rajesh M, Batkai S, Kechrid M, et al. Cannabinoid 1 receptor promotes cardiac dysfunction, oxidative stress, inflammation, and fibrosis in diabetic cardiomyopathy. Diabetes 2012;61: 716–27. [PubMed: 22315315]
8. Horti AG, Fan H, Kuwabara H, et al. 11CJHU75528: a radiotracer for PET imaging of CB1 cannabinoid receptors. J Nucl Med 2006;47: 1689–96. [PubMed: 17015906]
9. Wong DF, Kuwabara H, Horti AG, et al. Quantification of cerebral cannabinoid receptors sub-type 1 (CB1) in healthy subjects and schizophrenia by the novel PET radioligand [11C]OMAR. Neuro-image 2010;52:1505–13. [PubMed: 20406692]
10. Treyer V, Streffer J, Wyss MT, et al. Evaluation of the metabotropic glutamate receptor subtype 5 using PET and 11C-ABP688: assessment of methods. J Nucl Med 2007;48:1207–15. [PubMed: 17574984]

11. Fukushima K, Bravo PE, Higuchi T, et al. Molecular hybrid positron emission tomography/computed tomography imaging of cardiac angiotensin II type 1 receptors. J Am Coll Cardiol 2012; 60:2527–34. [PubMed: 23158533]
12. Kruse MJ, Kovell L, Kasper EK, et al. Myocardial blood flow and inflammatory cardiac sarcoidosis. J Am Coll Cardiol Img 2017;10:157–67.
13. Mukhopadhyay P, Batkai S, Rajesh M, et al. Pharmacological inhibition of CB1 cannabinoid receptor protects against doxorubicin-induced cardiotoxicity. J Am Coll Cardiol 2007;50:528–36. [PubMed: 17678736]
14. Terry GE, Liow JS, Zoghbi SS, et al. Quantitation of cannabinoid CB1 receptors in healthy human brain using positron emission tomography and an inverse agonist radioligand. Neuroimage 2009;48:362–70. [PubMed: 19573609]
15. Tsujikawa T, Zoghbi SS, Hong J, et al. In vitro and in vivo evaluation of (11)C-SD5024, a novel PET radioligand for human brain imaging of cannabinoid CB1 receptors. Neuroimage 2014;84: 733–41. [PubMed: 24076222]
16. Naya M, Tsukamoto T, Morita K, et al. Myocardial beta-adrenergic receptor density assessed by 11C-CGP12177 PET predicts improvement of cardiac function after carvedilol treatment in patients with idiopathic dilated cardiomyopathy. J Nucl Med 2009;50:220–5. [PubMed: 19164238]

PERSPECTIVES

COMPETENCY IN MEDICAL KNOWLEDGE:

[^{11}C]-OMAR PET/CT can identify up-regulation of myocardial CB1-R, which could reflect a mechanistic link in mediating heart failure in AOB.

COMPETENCY IN PATIENT CARE AND PROCEDURAL SKILLS:

Sequential application of [^{11}C]-OMAR PET/CT to assess myocardial CB1-R expression may represent a unique tool to monitor and guide treatment options in subjects with AOB that could lead to improved clinical outcomes, and further investigations are needed.

TRANSLATIONAL OUTLOOK:

[^{11}C]-OMAR positron emission tomographic/computed tomographic assessment of myocardial CB1-R expression up-regulation may reflect a novel biomarker of cardiac risk to develop heart failure and to predict its response to preventive treatment intervention. Specific CB1-R blockade and visualization with [^{11}C]-OMAR or other evolving radiotracer ligands and PET may hold promise to further optimize and individualize medical care in the prevention of obesity-related cardiomyopathy.

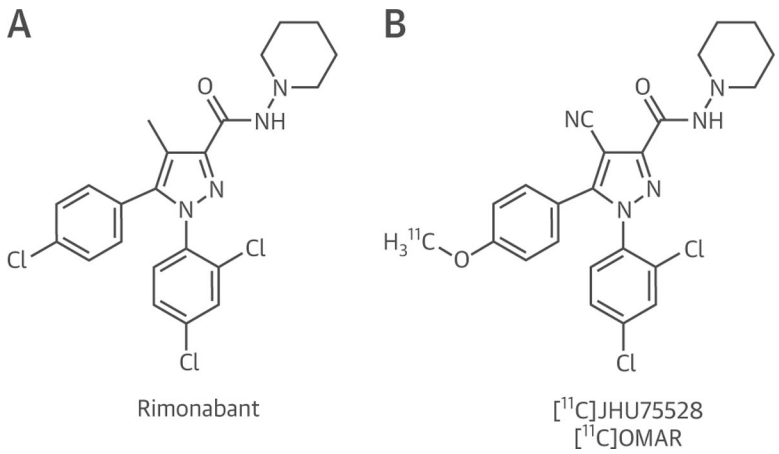

FIGURE 1. Chemical Structures

Chemical structure of the cannabinoid type 1 receptor inverse agonist rimonabant **(A)** and the radioligand [^{11}C]-OMAR **(B)**.

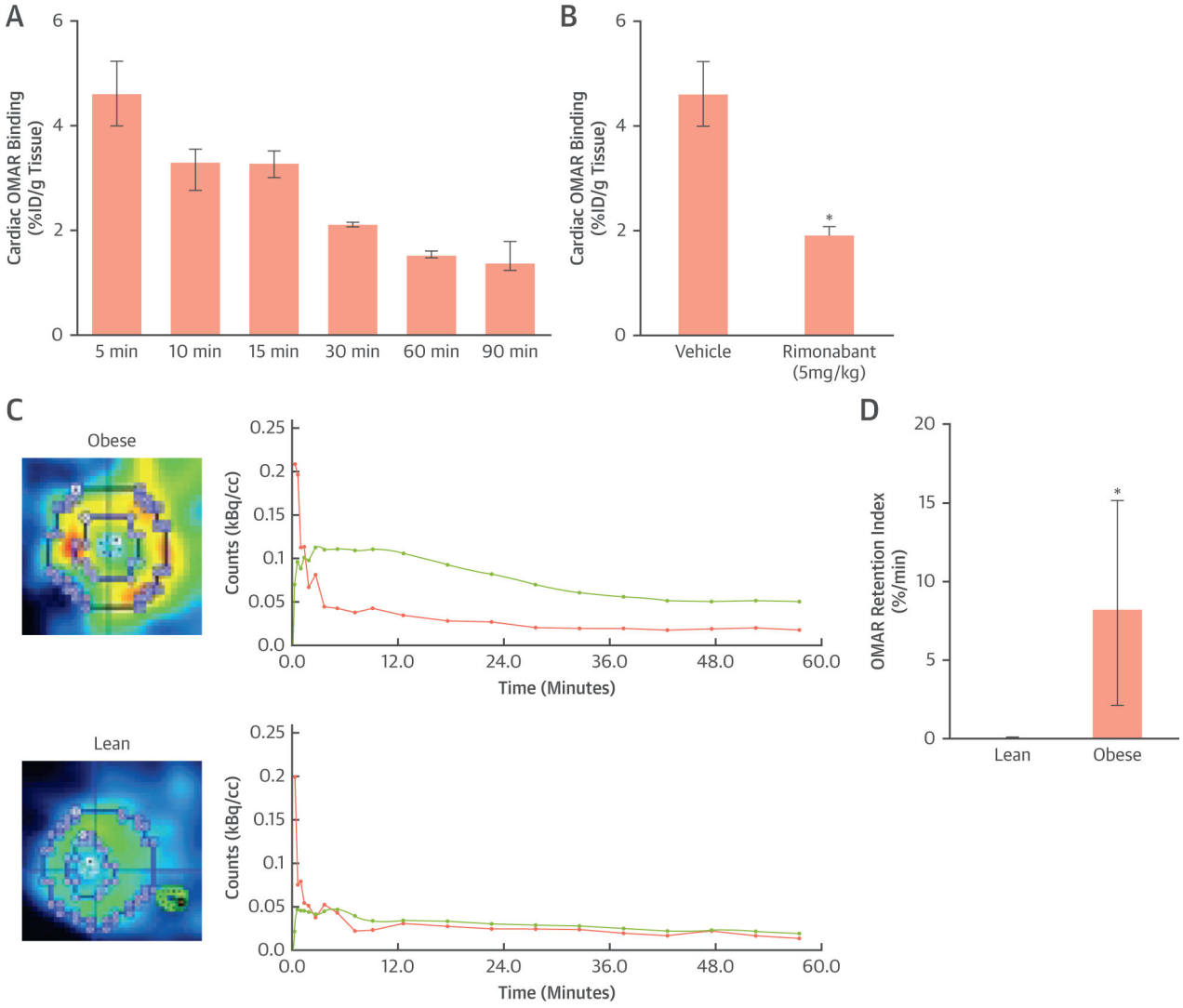

FIGURE 2. Myocardial [^{11}C]-OMAR Blocking Study and Imaging in Mice

Time course of cardiac OMAR binding **(A)** (n = 3 at each time point) and reversal at peak effect at 5 min with the cannabinoid type 1 receptor (CB1-R) antagonist rimonabant (5 mg/kg) in mice **(B)** (n = 3, respectively); *p ≤ 0.05. **(C)** Transaxial fusion micro–positron emission tomographic/computed tomographic image applying the CB1-R ligand [^{11}C]-OMAR in an obese mouse. Corresponding myocardial kinetics of [^{11}C]-OMAR **(top right)** with time-activity curves (TACs) for arterial blood pool **(pink)** and myocardium **(green)**. Transaxial fusion micro–positron emission tomographic/computed tomographic image of left ventricular [^{11}C]-OMAR uptake in a lean mouse **(bottom left)** and corresponding TACs **(bottom right)**. As can be appreciated, there is relatively higher [^{11}C]-OMAR myocardial uptake in the obese compared with the lean mouse. This is also reflected by a higher TAC course in the obese than in the lean mouse. **(D)** Quantitative analysis of myocardial OMAR retention index as a noninvasive probe of CB1-R binding in lean and obese mice (n = 5 and n = 7, respectively); *p ≤ 0.05. Bar graph: whisker length defines the range between smallest and largest observations. %ID = percentage of injected does.

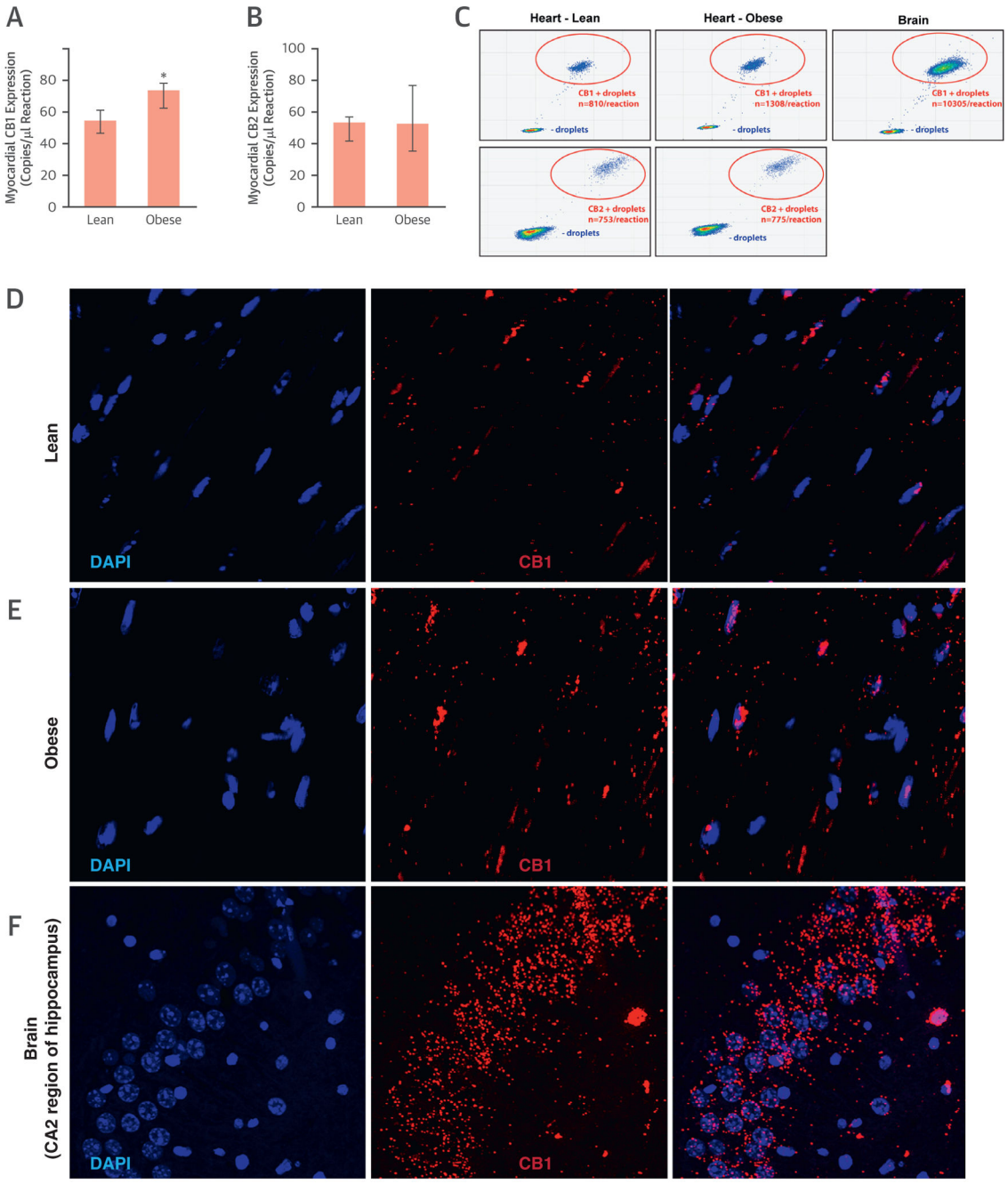

FIGURE 3. Myocardial Cannabinoid Type 1 Receptor Expression in Mice

(A) Expression of myocardial cannabinoid receptor type 1 (CB1-R), expressed as copies per microliter of the droplet digital polymerase chain reaction (ddPCR) in lean and obese mice (n = 3); *p ≤ 0.05. **(B)** Expression of myocardial cannabinoid receptor type 1 (CB2-R), expressed as copies per microliter of the ddPCR in lean and obese mice. **(C)** Representative ddPCR fluorescence-activated cell sorting plots of CB1-R and CB2-R expression in hearts of lean and obese mice and in the mouse brain (positive control for CB1-R) **(B)**. Each panel represents a single ddPCR experiment whereby a deoxyribonucleic acid sample was

segregated into individual droplets and assessed for the presence of CB1-R and CB2-R complementary deoxyribonucleic acid. Droplets in the **bottom left quadrant** represent negative droplets, while droplets in the **top right quadrant** are positive droplets, each droplet containing a single copy of the CB1-R and CB2-R, respectively. Confocal microscopic imaging of CB1-R messenger ribonucleic acid (mRNA) by RNAscope in situ hybridization in lean **(D)** and obese **(E)** mouse hearts, as well as in the CA2 region of mouse hippocampus **(F)**. 4′,6-Diamidino-2-phenylindole (DAPI) staining **(blue)** shows nuclear structure, and CB1 staining (Cy3; **red**) shows localization of CB1 mRNA.

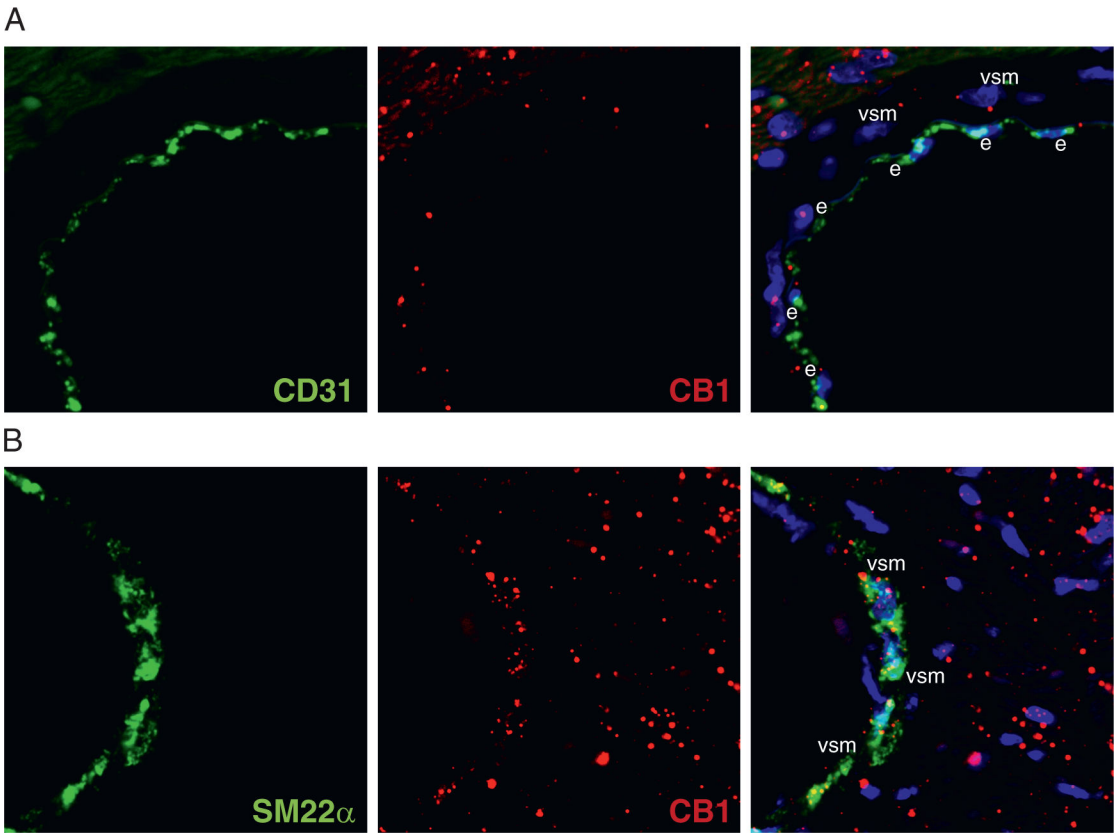

FIGURE 4. Colocalization of Cannabinoid Type 1 Receptor Messenger Ribonucleic Acid With Endothelial and Vascular Smooth Muscle–Specific Markers in Mice

(A) Confocal microscopic imaging of cannabinoid type 1 receptor (CB1-R) messenger ribonucleic acid (mRNA) **(red)** by RNAscope in situ hybridization with the endothelial marker CD31 **(green)** in obese mouse hearts. **(B)** Confocal microscopic imaging of CB1-R mRNA **(red)** by RNAscope in situ hybridization with the vascular smooth muscle–specific marker Sm22α **(green)** in obese mouse hearts. On the merged images, 4′,6-diamidino-2-phenylindole staining **(blue)** shows nuclear structure. e = endothelium; vsm = vascular smooth muscle.

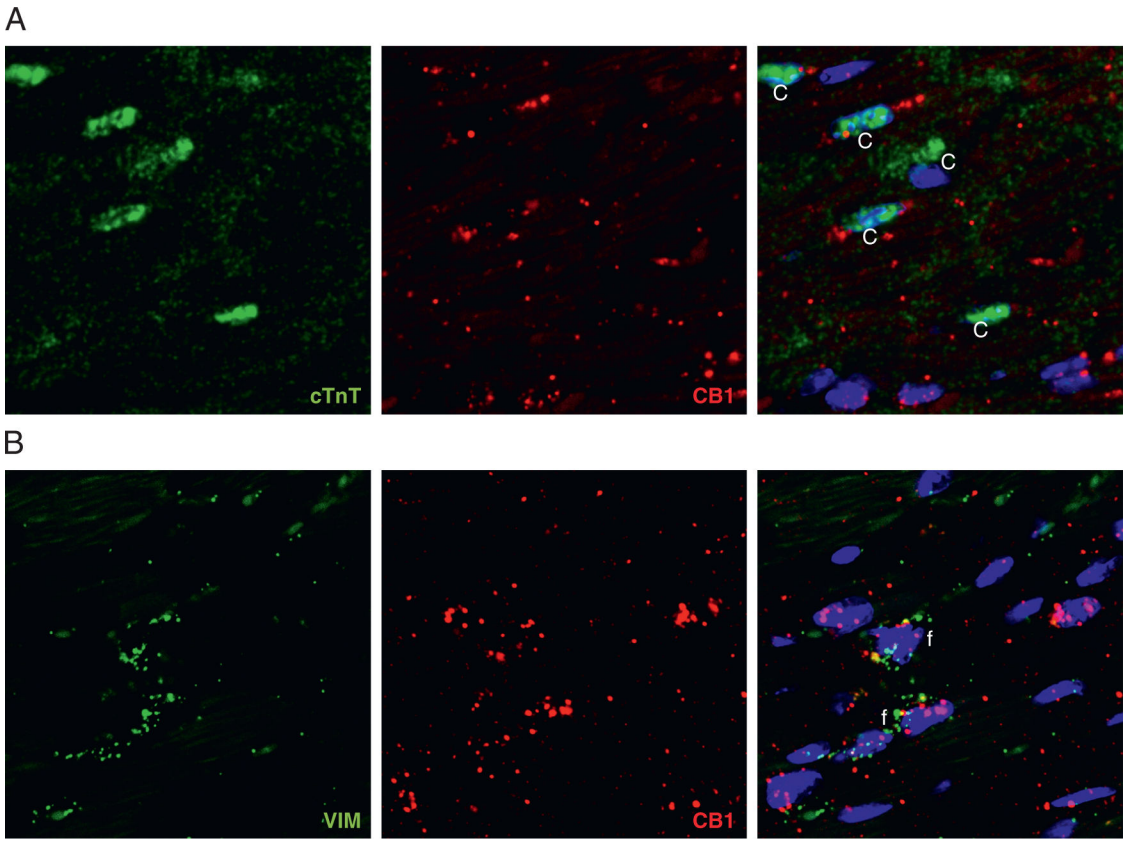

FIGURE 5. Colocalization of Cannabinoid Type 1 Receptor Messenger Ribonucleic Acid With Cardiomyocyte- and Fibroblast-Specific Markers in Mice

(A) Confocal microscopic imaging of cannabinoid type 1 receptor (CB1-R) messenger ribonucleic acid (mRNA) **(red)** by RNAscope in situ hybridization with the cardiomyocyte-specific marker cardiac troponin T (cTnT) **(green)** in obese mouse hearts. **(B)** Confocal microscopic imaging of CB1-R mRNA **(red)** by RNAscope in situ hybridization with the fibroblast-specific marker vimentin **(green)** in obese mouse hearts. On the merged images, 4′,6-diamidino-2-phenylindole staining **(blue)** shows nuclear structure.

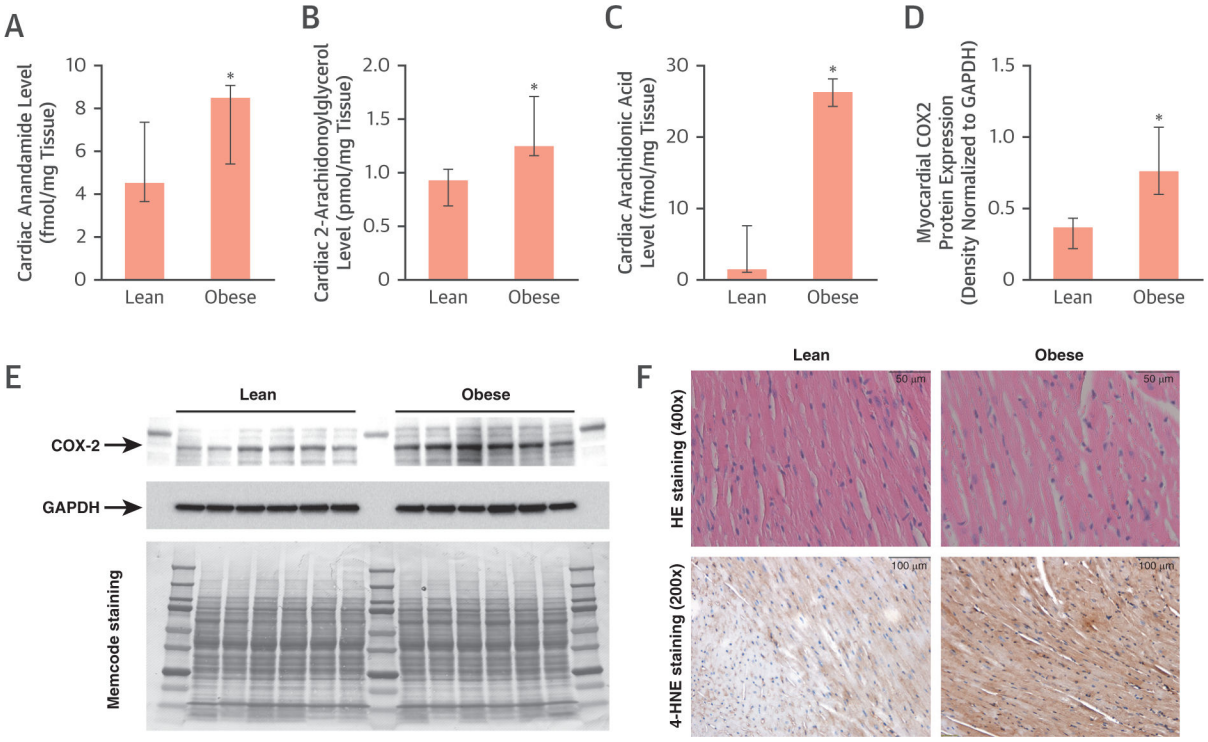

FIGURE 6. Myocardial Endocannabinoid Levels in Mice

Anandamide **(A)**, 2-arachidonoylglycerol (2-AG) **(B)**, and arachidonic acid **(C)** levels in hearts of lean and obese mice (n = 5); *p ≤ 0.05. **(D and E)** Expression of the arachidonic acid–metabolizing enzyme cyclooxygenase 2 (COX2) normalized to glyceraldehyde-3-phosphate dehydrogenase (GAPDH) as a loading control (n = 6);*p ≤ 0.05. Memcode staining shows equal total protein loading. **(F)** Representative histological sections from lean and obese mouse hearts and immunohistochemcial staining for the lipid-peroxidation marker 4-hydroxynonenal (4-HNE). HE = hematoxylin and eosin.

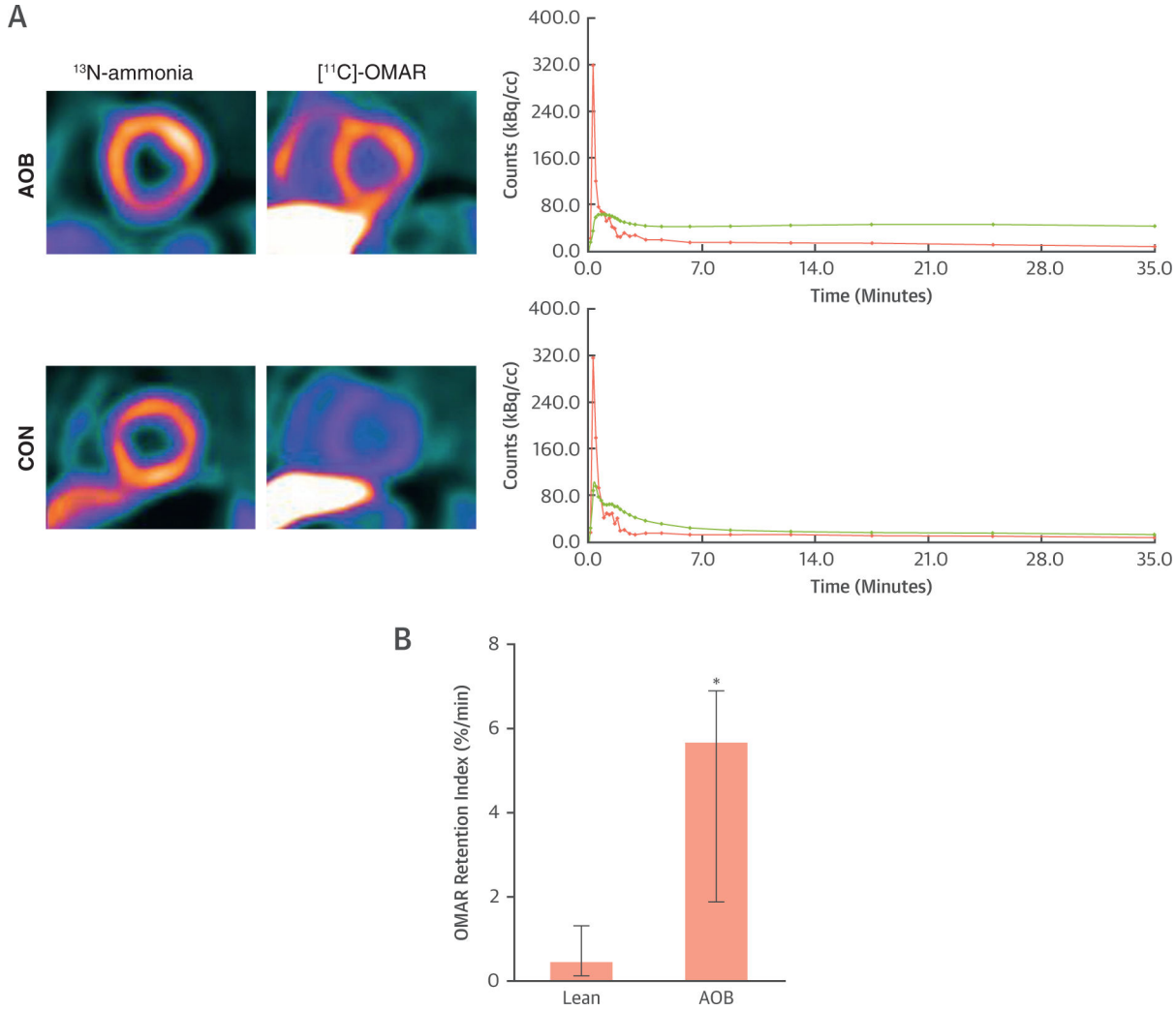

FIGURE 7. Myocardial Cannabinoid Type 1 Receptor Imaging Study in Humans

(A) Short-axis positron emission tomographic/computed tomographic image **(top left)** of the left midventricular myocardium using the cannabinoid type 1 receptor (CB1-R) ligand [^{11}C]-OMAR in a healthy subject with advanced obesity (AOB). Corresponding myocardial kinetics of [^{11}C]-OMAR **(top right)** with time-activity curves (TACs) for arterial blood pool **(pink)** and myocardium **(green)**. Furthermore, short-axis positron emission tomographic/computed tomographic image of the left midventricular myocardium in a healthy lean participant as a control subject (CON) **(bottom left)** and corresponding TAC **(bottom right)**. Also here, there is relatively higher [^{11}C]-OMAR myocardial uptake in a subject with AOB compared with lean CON that is mirrored by corresponding myocardial TAC course. **(B)** Quantitative analysis of myocardial OMAR retention index in humans with normal weight or CON and in subjects with AOB (n = 5 and n = 7, respectively); *p ≤ 0.05.

TABLE 1

Characteristics of the Study Population, OMAR Retention, and Hemodynamic Parameters During Positron Emission Tomography/Computed Tomography

	CON	AOB	*p* Value
Age, yrs	50 (47–65)	47 (24–55)	0.101
Female/male	2/3	3/4	–
BMI, kg/m^2	25 (23–25)	39 (38–56)	0.0001
Waist, cm	80 (79–84)	134 (127–151)	0.0001
Waist/hip ratio	0.83 (0.81–0.83)	1.05 (0.96–1.09)	0.0001
Cholesterol, mg/dl	180 (170–211)	168 (155–183)	0.087
LDL, mg/dl	115 (110–144)	97 (88–123)	0.048
HDL, mg/dl	43 (41–47)	39 (37–44)	0.032
Triglyceride, mg/dl	77 (56–109)	93 (77–116)	0.254
Glucose, mg/dl	93 (80–102)	109 (82–114)	0.119
C-reactive protein, mg/dl	1.6 (0.9–2.1)	6.5 (3.1–12.1)	0.004
Hemodynamic parameters before [^{11}C]-OMAR injection			
HR, beats/min	67 (55–84)	72 (55–90)	0.511
SBP, mm Hg	125 (116–133)	133 (110–137)	0.520
DBP, mm Hg	61 (55–72)	71 (52–90)	0.259
RPP, mm Hg/min	8,710 (6,490–11,172)	9,520 (7,315–10,720)	0.486
MAP, mm Hg	82 (75–92)	92 (71–106)	0.318
Hemodynamic parameters after [^{11}C]-OMAR injection			
HR, beats/min	70 (61–77)	72 (65–84)	0.763
SBP, mm Hg	120 (118–124)	133 (116–140)	0.226
DBP, mm Hg	62 (60–68)	71 (56–78)	0.353
RPP, mm Hg/min	8,260 (7,15–11,730)	9,588 (7,325–10,960)	0.538
MAP, mm Hg	81 (75–97)	93 (76–96)	0.286
OMAR retention, %/min	0.47 (0.13–1.31)	5.68 (1.88–6.89)	0.006
MBF, ml/g/min	0.67 (0.60–0.88)	0.74 (0.60–0.95)	0.396
NMBF, ml/g/min	0.73 (0.63–1.57)	0.92 (0.60–1.13)	0.913
CVR, mm Hg/ml/min	117 (86–149)	120 (81–142)	0.766
LVEF, %	62 (50–63)	52 (51–61)	0.092
EDV, ml	128 (72–135)	116 (84–146)	0.502
ESV, ml	50 (25–66)	57 (32–71)	0.249
SV, ml	62 (48–83)	60 (52–78)	0.992
PFR, s	1.87 (1.76–2.22)	1.78 (1.44–2.58)	0.796
TPFR, s	137 (133–169)	155 (135–181)	0.317
1/3 MFR, s	1.29 (1.12–1.44)	1.14 (1.11–1.42)	0.184

Values are median (range) or n.

AOB = advanced obesity; BMI = body mass index; CON = control; CVR = coronary vascular resistance; DBP = diastolic blood pressure; EDV = end-diastolic volume; ESV = end-systolic volume; HDL = high-density lipoprotein; HR = heart rate; LDL = low-density lipoprotein; LVEF = left ventricular ejection fraction; MAP = mean arterial pressure; MBF = myocardial blood flow; MFR = mean filling rate; NMBF = normalized

myocardial blood flow; PFR = peak filling rate; RPP = rate-pressure product; SBP = systolic blood pressure; SV = stroke volume;TPFR = time to peak filling rate.

TABLE 2

Time Course of [^{11}C]-OMAR Uptake in the Heart, Blood, and Different Brain Regions

	[^{11}C]-OMAR (%ID/g Tissue)					
	5 min	**10 min**	**15 min**	**30 min**	**60 min**	**90 min**
Heart	4.63 (4.00–5.23)	3.31 (3.01–3.52)	3.31 (3.01–3.52)	2.14 (2.09–2.17)	1.55 (1.48–1.61)	1.40 (1.40–1.79)
Blood	1.19 (1.10–1.33)	0.99 (0.91–1.19)	0.99 (0.91–1.19)	0.55 (0.39–0.65)	0.46 (0.46–0.47)	0.55 (0.51–0.68)
Cerebellum	2.43 (1.72–2.74)	2.32 (2.11–2.50)	2.53 (2.43–2.55)	2.11 (1.25–2.38)	1.37 (1.25–1.51)	1.11 (1.05–2.00)
Thalamus	1.78 (1.25–1.93)	1.62 (1.59–1.72)	1.69 (1.59–1.72)	1.21 (1.18–1.21)	0.73 (0.58–0.77)	0.55 (0.38–0.98)

Values are median (range).

%ID = percentage of injected dose.

TABLE 3

Rimonabant Blocking Study of [^{11}C]-OMAR Uptake in the Heart, Blood, and Different Brain Regions

	[^{11}C]-0MAR (%ID/g Tissue)		
	Vehicle	**Rimonabant 1 mg**	**Rimonabant 5 mg**
Heart	4.63 (4.00–5.23)	5.11 (3.68–6.99)	1.94 (1.91–2.15)
Blood	1.19 (1.10–1.33)	1.99 (1.08–2.16)	0.54 (0.38–0.72)
Cerebellum	2.43 (1.72–2.74)	1.50 (1.43–1.78)	0.79 (0.78–0.80)
Thalamus	1.78 (1.25–2.07)	1.33 (1.24–1.49)	0.57 (0.22–0.63)

Values are median (range).

%ID = percentage of injected dose per gram of tissue;

vehicle = mouse without rimonabant application.